Journal of Alloys and Compounds 504 (2010) 420–426

Contents lists available at ScienceDirect

Journal of Alloys and Compounds

journal homepage: www.elsevier.com/locate/jallcom

The role of doping on the structural and functional properties of $BiFe_{1-x}Mn_xO_3$ magnetoelectric ceramics

Adelina Ianculescu [a], Felicia Prihor Gheorghiu [b,*], Petronel Postolache [b], Ovidiu Oprea [a], Liliana Mitoseriu [b]

[a] Dept. of Science & Engineering of Oxide Materials, Polytechnics University of Bucharest, Romania
[b] Dept. of Physics, Al. I. Cuza University, Bv. Carol I no. 11, Iasi, 700506, Romania

ARTICLE INFO

Article history:
Received 17 February 2010
Received in revised form 28 May 2010
Accepted 28 May 2010
Available online 10 June 2010

Keywords:
Ceramics
Solid state reaction
Microstructure
Dielectric response

ABSTRACT

$BiFeO_3$ is one of the few single-phase multiferroics, showing antiferromagnetic and ferroelectric ordering. Since the dielectric properties in the ceramic state of the pure $BiFeO_3$ were rather poor and in order to stabilize the perovskite state and to induce ferromagnetism at room temperature, it was adopted the strategy of doping with rare earth or forming solid solutions. Substituting Fe with Mn in $BiFeO_3$-based compounds is supposed cause better properties in terms of leakage current density and also to induce changes in the magnetic order of the system. In the present paper, the effect of Mn substitution on the dielectric and magnetic properties of the $BiFe_{1-x}Mn_xO_3$ ceramics has been studied. Homogeneous samples from microstructural point of view were obtained for all the compositions analyzed. The magnetic properties are strongly affected by the presence of Mn ions. The possible origin of these behavior is discussed in terms of phase purity, grain size and grain boundary phenomena. The extrinsic properties are impossible to be fully controlled by normal ceramic processing. By controlling the extrinsic contributions to the dielectric properties, the ceramic system might be a valuable multiferroic material for magnetoelectric applications. At room temperature the ceramic is a multiferroic, since it is ferroelectric and magnetically-ordered.

1. Introduction

Multiferroic materials, in which ferroelectricity and magnetism coexist, attract much attention from both fundamental and practical points of view [1,2]. Although multiferroics are highly exciting materials for potential application, there are few systems which show magnetoelectric (ME) multiferroic behavior, due to the apparent opposite requirements concerning the d-orbital occupancy for ferroelectric and magnetic order [3,4].

$BiFeO_3$ (BFO) is one of the few single-phase multiferroics at room temperature having a distorted perovskite structure with rhombohedral symmetry (space group *R*3c). It exhibits both ferroelectric properties with a high Curie temperature (T_C = 830 °C) and antiferromagnetic order (Néel temperature T_N = 370 °C), and also shows a weak ferro/ferri magnetic characteristic in some temperature ranges [5]. Although promising for its multiferroic character, only poor dielectric and ferroelectric properties (low values of the polarization and of the dielectric constant) were found at room temperature in the bulk ceramics, mainly due to the semiconducting character which does not allow a proper electrical poling and lead to high dielectric losses [4].

In order to improve the electrical properties while preserving the magnetic ordering, several research groups adopted the strategy of doping $BiFeO_3$ with different +3 valence ions on A, B or both A and B sites [6–10]. The doping has resulted in the reduction of the leakage current density and in the improvement of the ferroelectric properties to some extent. Such substitutions were also expected to shift the transition temperature towards the room temperature. According to the Shannon et al. [11], the Mn^{3+} (ionic radius = 0.645 Å) ions can occupy the Fe^{3+} sites in $BiFeO_3$ materials, because both ions have the same valence state and similar ionic size to that of Fe^{3+} (0.645 Å). Even if there are different oxidation states of Mn (3+, 4+) in Mn-doped $BiFeO_3$ materials, the ionic radii of the different oxidation states of Mn are comparable to that of Fe^{3+}. Consequently, the Mn ions can occupy the Fe sites only. Similar types of observations have been reported by Chung et al. [8].

From technological point of view, magnetoelectric multiferroics are wanted to show a kind of magnetic order (ferro- or ferrimagnetic) at room temperature. Due to the cycloidal spin magnetic structure [12] with long wavelength (~62 nm), a weak ferromagnetism was generally observed in $BiFeO_3$ at room temperature. In addition, weak ME coupling is often reported. The substitution of Fe with Mn in $BiFeO_3$-based compounds is expected to result in better

* Corresponding author.
E-mail address: felicia_prihor@stoner.phys.uaic.ro (F.P. Gheorghiu).

0925-8388/$ – see front matter © 2010 Elsevier B.V. All rights reserved.
doi:10.1016/j.jallcom.2010.05.135

properties in terms of reducing the leakage current and to induce ferromagnetic properties. The magnetic moment and anisotropy were reported to increase by substituting other 3d transition atoms for the iron atoms at B sites of $BiFeO_3$, due to the differences in the magnetic moments among the B sites, which induced either a local ferrimagnetic spin configuration, a complex chiral spin structure, or changes in the gradient of spin canting [13]. A small enhancement in magnetization in Mn-doped $BiFeO_3$ was also reported as result of the modification of the oxidation state of Fe ion [14].

In the present work, the effect of Mn—substitution on the functional properties of the $BiFeO_3$ ceramics prepared by mixed oxides reaction was investigated.

2. Experimental

The $BiFe_{1-x}Mn_xO_3$ solid solutions ($0 \le x \le 0.40$) were prepared by solid state reaction from high purity oxides: Bi_2O_3 (Fluka), Fe_2O_3 (Riedel de Haen) and MnO_2 (Merck), by using a two-step thermal treatment procedure, consisting of presintering of the compacts at 650 °C for 2 h followed by grinding, reshaping, sintering at 850 °C for 2 h with a heating rate of 5 °C/min and the slow cooling, as described in detail in the ref. [15]. The place of the selected compositions in the ternary Bi_2O_3–Fe_2O_3–Mn_2O_3 system is presented in Fig. 1.

The phase composition at different calcinations steps and after sintering was checked with a SHIMADZU XRD 6000 diffractometer using Ni-filtered CuKα radiation, $\lambda = 1.5418$ Å, with scan step increments of 0.02° and counting time of 1 s/step, for 2θ, ranged between 20° and 80°. To estimate the structural characteristics, the same step increment but with a counting time of 10 s/step, for 2θ ranged between 20° and 120° was used. Parameters to define the position, magnitude, shape and integral breadth or full width at half maximum of profile (FWHM) of the individual peaks are obtained using the pattern fitting and profile analysis of the original X-ray 5.0 program. The lattice constants calculation is based on the Least Squares Procedure (LSP) using the linear multiple regressions for several XRD lines, depending on the unit cell symmetry. To deconvolute size-D and strain-S broadening from the XRD spectra the multiple line analysis and integral breadth methods applied to the PVII analytic profiles was used.

DSC experiments were performed with a Netzsch TG 449C STA Jupiter. Ceramic powdered samples were placed in alumina crucible and heated with 10 °C min^{-1} from room temperature to 850 °C and back, under the flow of 20 mL min^{-1} dried Ar.

A HITACHI S2600N scanning electron microscope SEM coupled with EDX was used to analyze the ceramics microstructure and to check the chemical composition of the ceramic samples.

For the electrical characterization, Ag-electrodes were applied on the polished surfaces of the sintered ceramic disks. The dielectric measurements of the ceramic samples in the low frequency range 10–10^6 Hz were performed by using an Solartron 1260A Impedance/Gain-Phase Analyzer and at high frequency 10^6–10^9 Hz with an impedance/material analyzer type E4991A RF, at room temperature. The magnetic properties were determined with a Vibrating Sample Magnetometer MicroMag™ VSM model 3900 (Princeton Measurements Co.). The $M(H)$ magnetic loops of the solid solutions were determined at room temperature under magnetic fields in the range of 0–14 kOe.

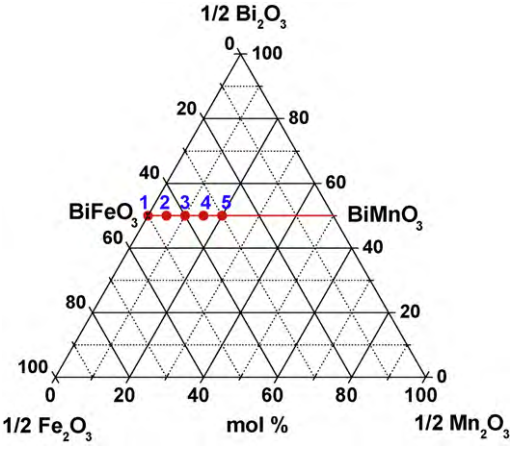

Fig. 1. Place of the selected compositions in the ternary Bi_2O_3–Fe_2O_3–Mn_2O_3 system: (1) $x = 0$, (2) $x = 0.10$, (3) $x = 0.20$, (4) $x = 0.30$, (5) $x = 0.40$.

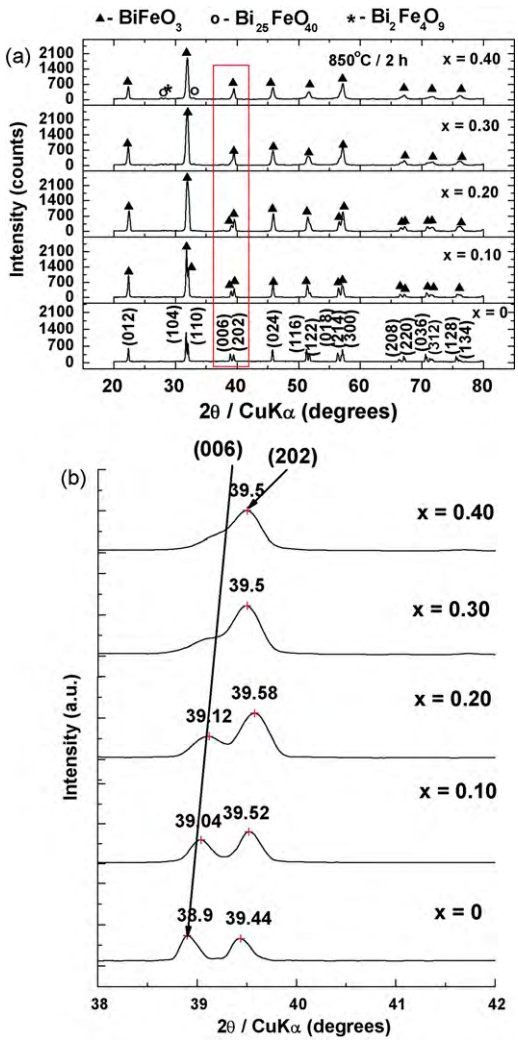

Fig. 2. (a) Room temperature XRD patterns of the $BiFe_{1-x}Mn_xO_3$ ceramics sintered at 850 °C/2 h; (b) detail—(rectangle of (a)).

3. Results and discussions

3.1. Phase composition and structure

The room temperature X-ray diffraction patterns recorded for the sintered samples show almost single phase compositions, consisting of the well-crystallized perovskite phase (Fig. 2(a)). Secondary phases, if present, are below the XRD instrumental detection limit of 3%. Only for the composition with $x = 0.40$, small amounts of secondary $Bi_{25}FeO_{40}$ and $Bi_2Fe_4O_9$ phases were identified.

From the structural point of view, the XRD data pointed out that all the samples investigated here exhibit hexagonal $R3c$ symmetry, similar to the structure of the paternal non-modified $BiFeO_3$ compound. In spite the increase of the manganese content does not induce a modification of the spatial group, certain distortions clearly emphasized by the cancellation of the splitting of some characteristic XRD peaks occur. Thus, Fig. 2(b) shows the evolution of the profile and position of the neighbouring (0 0 6) and (2 0 2) peaks specific to the undoped $BiFeO_3$ composition when manganese is added in the system. One can observe that an amount of 30% Mn replacing Fe^{3+} in the perovskite lattice determines the disappearance of the (0 0 6) peak in the characteristic XRD pattern.

The increase of the manganese concentration induces an obvious decrease of both a and c lattice parameters (Fig. 3(a)) and,

therefore, a gradual contraction of the unit cell volume is pointed out (Fig. 3(b)). These results are in good agreement with those reported by Palkar et al. [14] and by Sahu and Rao [16]. This evolution suggests that the $Mn^{3+} \leftrightarrow Fe^{3+}$ substitution is unlikely, because of the higher value of the Mn^{3+} ionic radius ($r(Mn^{3+}) = 0.645$ Å) in comparison with that one of Fe^{3+} ($r(Fe^{3+}) = 0.645$ Å), which normally should determine no variation of the lattice parameters with the increase of the manganese content. Taking into account that both manganese and iron are versatile species with multiple oxidation states, the following substitution mechanisms might be considered in order to explain the evolution of the unit cell parameters:

(i) the 2+ oxidation state of the iron ions prevails, so that the substitution $Mn^{3+} \leftrightarrow Fe^{2+}$ could explain the decrease of the unit cell parameters with the increase of the manganese content, due to the lower value of the Mn^{3+} ionic radius in comparison with the larger one of Fe^{2+} ($r(Fe^{2+}) = 0.78$ Å);
(ii) if we assume that the predominant oxidation state of the iron is 3+, than the most of the manganese ions are more likely incorporated on the B site of the perovskite network as Mn^{4+} ($Mn^{4+} \leftrightarrow Fe^{3+}$) causing the decrease of the network parameters because of the smaller ionic radius of Mn^{4+} (0.53 Å), in comparison with that one corresponding to Fe^{3+} (it is worthy to mention that all the values of the ionic radii (Shannon) were considered taking into account the octahedral coordination (CN = 6) of the Fe and Mn ions in the perovskite unit cell and assuming the high spin state of Fe^{3+}, Fe^{2+} and Mn^{3+} ions);
(iii) it cannot be excluded the hypothesis of a redox coupling between the iron ions which could be partially reduced on the expense of the oxidation of some of the manganese ions, according to the following equation:

$$Fe^{3+} + Mn^{3+} \leftrightarrow Fe^{2+} + Mn^{4+}$$

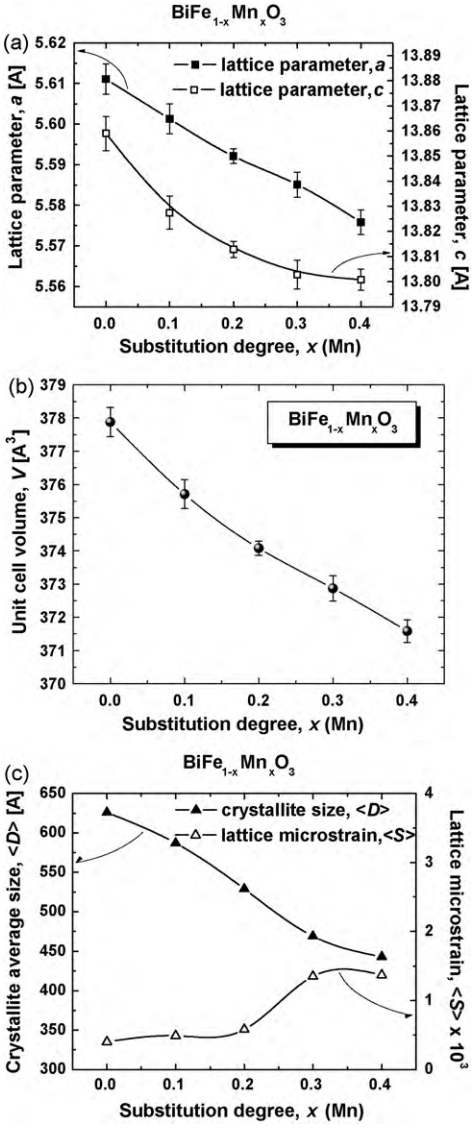

Fig. 3. Influence of the manganese content in $BiFe_{1-x}Mn_xO_3$ ceramics obtained after sintering at 850 °C for 2 h on the structural parameters: (a) lattice parameters; (b) unit cell volume and (c) crystallite average size and lattice microstrains.

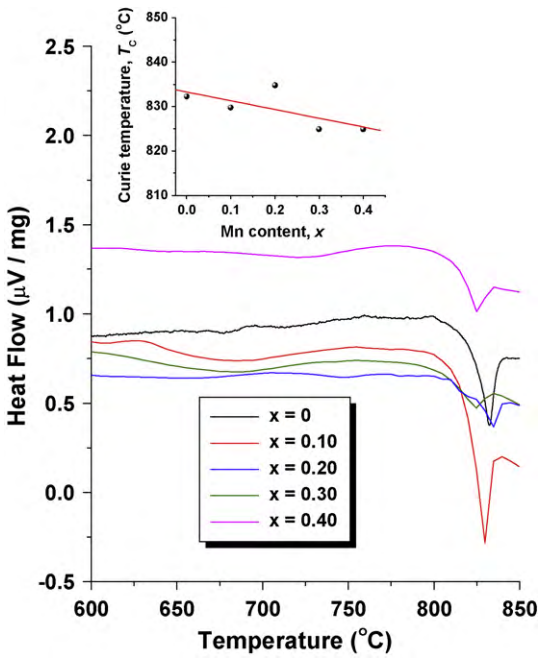

Fig. 4. High temperature DSC data for the $BiFe_{1-x}Mn_xO_3$ solid solutions (the inset shows the evolution of the ferroelectric–paraelectric transition temperature with the Mn content, as determined from the DSC endothermic peaks).

We considered that other higher (+7) or lower (+2) oxidation states for the manganese ions are unlikely, since the difference between the values of the related ionic radii and those corresponding to the iron species could not accommodate the perovskite structure. However, in order to determine the valence state of the iron and manganese ions and thereby to elucidate the substitution mechanisms which could take place, further XPS analyses are required.

The presence of the manganese solute on the Fe^{3+} sites influences also the crystallite average size, this one acting as an inhibitor. Thus, the higher the manganese content, the smaller are the crystallites in the ceramic bodies and consequently, the higher are the related lattice microstrains, as shown in Fig. 3(c).

In order to estimate the influence of the manganese content on the ferroelectric–paraelectric phase transition temperature, differential scanning calorimetry measurements were performed on the powder samples (Fig. 4). Well-marked phase transitions in the temperature range of 824–833 °C were pointed out by the DSC curves. An evolution characterized by a tendency to a non-monotonous decrease of the phase transition temperature against the Mn concentration is noticed (Fig. 4—inset). These results are in agreement with the DTA data reported by Sahu and Rao [16].

3.2. Microstructure

SEM investigation performed on the surface of the undoped $BiFeO_3$ ceramic sample pointed out a microstructure consisting of large, well-interlinked and non-uniform (as shape and size) grains and a certain intergranular porosity, which affects the sample density (Fig. 5(a)).

The addition of 10 at% manganese on the iron sites determines, from microstructural point of view, a significant decrease of the average grain size and the formation of a supplementary amount of interconnected pores by Kirkendall effect. Therefore, a porous microstructure which consists of agglomerates formed by a variable number of small grains (of 1–2 μm), without well defined grain boundaries was noticed (Fig. 5(b)).

The increase of the manganese concentration ($x = 0.20$) in the system seems to have a beneficial effect on the densification due to the decrease of the intergranular porosity, In this case, the grain size slightly increased (~5 μm) and the grains exhibit well-defined boundaries (Fig. 5(c)). Further increase of the solute content favors the coalescence of the small grains and consequently, the densification process is more obvious (Fig. 5(d)).

3.3. Dielectric properties

Low frequency dependence of the dielectric permittivity and loss factor at room temperature obtained for $BiFe_{1-x}Mn_xO_3$ are presented in Fig. 6. Very high values of permittivity in the range of 1000–30,000 are observed at low frequency, followed by a monotonous decrease with frequency at room temperature, for all the compositions (Fig. 6(a)). Losses above unity are characteristic for these ceramics, particularly at low frequency, for which $\tan\delta$ is about a few tenths (Fig. 6(b)). The losses also are strongly diminishing with increasing frequency and they reduce below unity for $f = 10^6$ Hz. This indicates that the high values of permittivity at low frequency are not intrinsic properties of the ceramic compounds, but they are rather related to conductive properties. The highest values of permittivity and losses are found for $x = 0.20$ and $x = 0.30$, as result of the highest conductivity among all the Mn-doped $BiFeO_3$ compositions. The frequency dependence of the real permittivity indicates the presence of a complex dielectric relaxation and/or conduction contributions.

Losses above unity (between 0 and 30) and the presence of the complex dielectric relaxation demonstrated by multiple maxima in the tangent loss (Fig. 6(c)) seem to be a result of locally uncompensated space charges giving rise to Maxwell–Wagner phenomena due to quasi-mobile carriers [17]. The impedance spectra of the ceramic samples (Fig. 6(c)) are characterized by more semicircular arcs, whose pattern changes with composition, indicating an impedance modification when increasing the Mn addition x. The presence of more than one component in the complex impedance plot demonstrated that the ceramic samples present some degree of local electrical heterogeneity even they are homogeneous from structural and compositional point of view, for all the degrees of Mn addition.

To understand this behavior, we have to note that even in pure $BiFeO_3$, small amounts of Fe^{2+} ions and oxygen vacancies exist [18]. $BiFeO_3$ shows p-type conductivity [19], which can be understood by considering the substitution of a small amount Fe^{2+} ions in Fe^{3+} positions (acceptor doping of Fe^{3+} by Fe^{2+}). Doped with Mn in various degrees of substitutions, both the mechanisms (i) and (ii) previously discussed might result in various amounts of oxygen vacancies. The oxygen vacancies are compensated by the incorporation of oxygen from the atmosphere mainly at the ceramic grain boundaries, according to the relation:

$$V_O^{\bullet\bullet} + (1/2)O_2(g) \Leftrightarrow O_O + 2h^{\bullet} \quad (1)$$

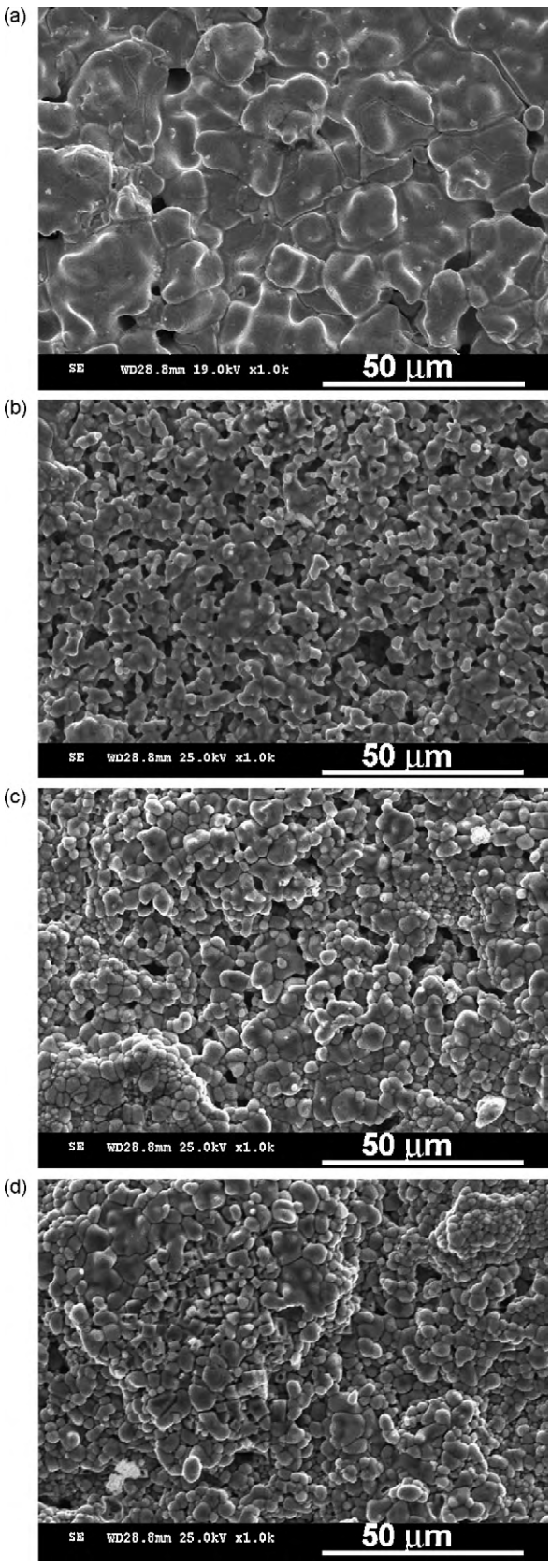

Fig. 5. Surface SEM images of the $BiFe_{1-x}Mn_xO_3$ ceramics obtained after sintering at 850 °C/2 h: (a) $x = 0$; (b) $x = 0.10$; (c) $x = 0.20$ and (d) $x = 0.30$.

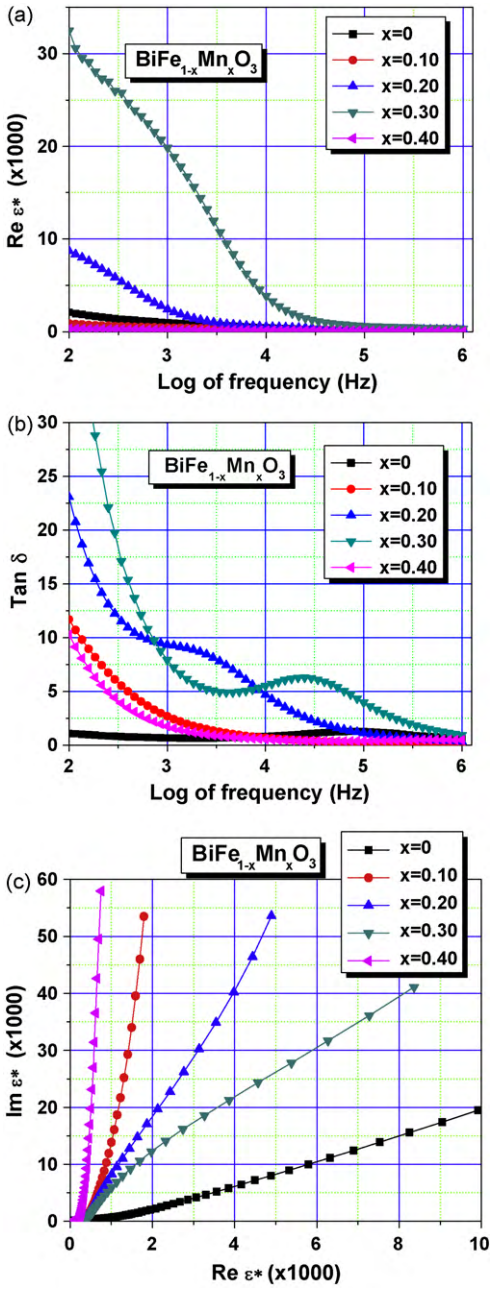

Fig. 6. Dielectric properties of the $BiFe_{1-x}Mn_xO_3$ ceramics at room temperature in the frequency range 10^2–10^6 Hz: (a) real part of permittivity *vs.* frequency; (b) tangent loss *vs.* frequency and (c) complex impedance plot.

and produce p-type conductivity. The hole generated can be consumed by Fe^{2+} in Fe^{3+} positions [20] as:

$$2Fe^{2+}_{Fe^{3+}} + 2O_O + O_O + 2h^{\bullet} \Leftrightarrow 2Fe^{3+}_{Fe^{3+}} + 3O_O \quad (2)$$

resulting in lower acceptor doping of Fe^{3+} by Fe^{2+} in $BiFeO_3$, or by Mn^{4+} in Mn^{3+}, with a subsequent decrease in conductivity, particularly at the ceramic grain boundaries. In any case, a difference between the conductivity inside the ceramic grains and on the grain boundary most probably exists, which also causes a complex dielectric relaxation behavior. Inside the ceramic grain, the level of oxygen vacancies is higher than at the boundary. The contribution of oxygen vacancies to the dielectric response can be 3-fold:

(a) it can hop in the lattice, leading to the associated dipolar moment reorientation [21];

(b) it creates conducting electrons through the ionizations:

$$V_O \Leftrightarrow V_O^{\bullet} + e', \; V_O^{\bullet} \Leftrightarrow V_O^{\bullet\bullet} + e', \quad (3)$$

the conducting electrons in their turn can hop from one localized state to another one in the lattice, equivalent to the reorientation of effective electric dipoles [22,23];

(c) different levels of oxygen deficiency in different spatial regions within the sample lead to electric heterogeneity even in single phase materials, leading to interfacial polarization (Maxwell–Wagner or space charge relaxation mechanism) [24–26]. The grain boundary in polycrystalline ceramics and various defect structures (such as twin boundaries, dislocations) in single crystals and interphases in composites play an important role in this mechanism. All of these effects create a complex dielectric behavior with multiple relaxation and conduction components, which might be different according to the degree of substitutions and microstructural characteristics of each of the present Mn-doped $BiFeO_3$ ceramics.

In any case, it seems that the Mn-doping of $BiFeO_3$ did not result in improving the low field permittivity and losses by comparison with pure $BiFeO_3$ ceramics. Similar observation was reported for the addition of Mn, Co, and Cu to the $BiFeO_3$ films, for which an effective reducing of the leakage current density in the high electric field region was only found [13]. Opposite, it seems that the Mn-addition increased the degree of local electrical heterogeneity, resulting in more complex impedance spectra.

For understanding which mechanism plays the main role in the complex dielectric response of these ceramics, the dielectric modulus was also investigated and will be discussed in the following.

From the physical point of view, electrical modulus corresponds to the relaxation of the electric field in the material when the electric displacement is maintained as constant [27,28]. The usefulness of the modulus representation in the analysis of relaxation properties was demonstrated for various ionic conductors and polycrystalline ceramics [29]. The variation of its imaginary component as a function of frequency $M''(f)$ at room temperature provides useful information concerning the charge transport mechanism such as conductivity relaxation. A conductivity relaxation is indicated by the presence of a peak in the $M''(f)$ spectra and no peak would take place in the corresponding plot of $\varepsilon''(f)$, while the dielectric relaxation gives maxima both in the imaginary part of permittivity $\varepsilon''(f)$ and of the dielectric modulus $M''(f)$ spectra. Comparisons of the complex ε^* and M^* representations have been used to distinguish localized dielectric relaxation processes from long-range conductivity [30,31].

In the low frequency range, the ceramics show at least one maximum of the imaginary part $M''(f)$ (Fig. 7(a)) and apparently no peak in the imaginary part $\varepsilon''(f)$ excepting the very-low frequency range (Fig. 7(b)), which confirm the proposed conductivity relaxation mechanism. The comparative frequency-dependent conductivity results presented in the (Fig. 7(c)) at room temperature show an almost zero conduction at low frequency (up to 100 kHz) with a large increasing for the frequency range 10^5–10^6 Hz, for all the compositions excepting $x = 0.30$. This composition, followed by $x = 0.20$ also presented the highest losses at low frequency (Fig. 6(b)), which are due to dc-conductivity mechanisms. The mechanism causing the highest dc-conductivity and losses for these compositions is not yet clear.

If the low-frequency range seems to be dominated by important contributions from the dc-conductivity, possible improving of the

dielectric characteristics might be achieved at higher frequencies. The experiments performed in the frequency range of 10^6–10^9 Hz, show a reducing permittivity with increasing frequency and some dielectric relaxations (Fig. 8).A tendency towards small permittivity values of units (in the range of 2.5–7.5) are found for 10^9 Hz, which can be considered as intrinsic permittivity values for these compounds. Losses due to the dc-conductivity, typical at low frequencies, are strongly reduced, but $\tan\delta$ is still above unity in some frequency ranges (Fig. 8(b)). The degree of doping does not seem to change dramatically the general dielectric behavior, even at high frequencies. However, the compositions $x = 0.10$, 0.20 and 0.30 show dielectric losses below unity in the high frequency range (Fig. 8(b)), making these compositions as acceptable from dielectric point of view at such frequency. The complex dielectric behavior is observed even in the low-permittivity range (high frequencies), for which more than one component are again obtained (Fig. 8(c)).

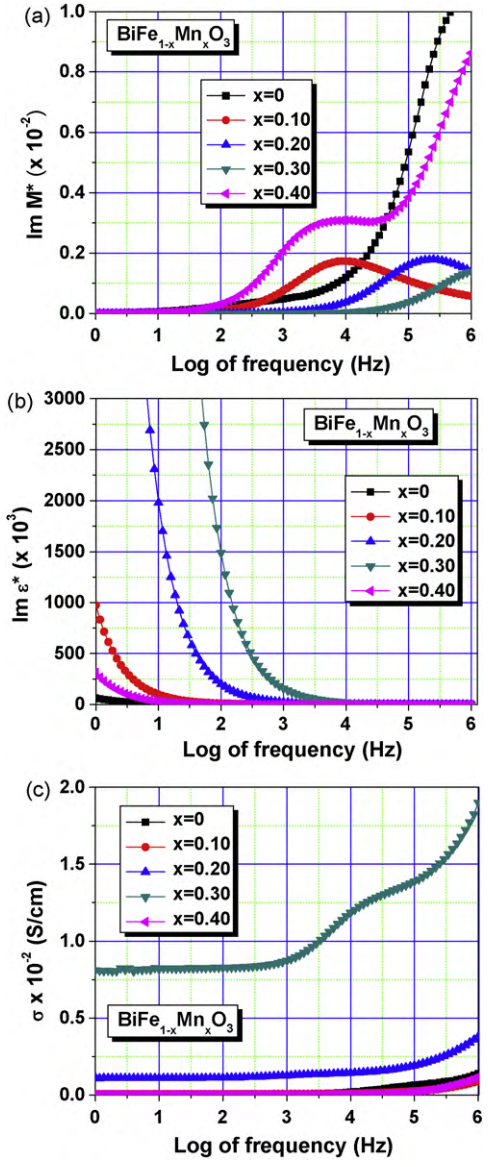

Fig. 7. The complex dielectric response of the $BiFe_{1-x}Mn_xO_3$ samples at room temperature: (a) frequency dependence of the imaginary part of the dielectric modulus M^*; (b) frequency dependence of the imaginary part of the permittivity and (c) frequency dependence of the effective conductivity.

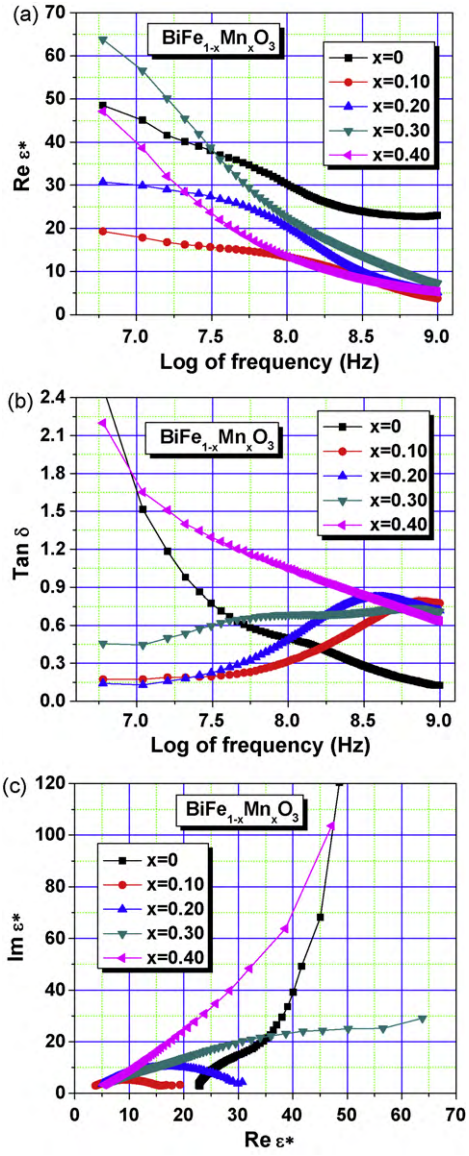

Fig. 8. Dielectric properties of the $BiFe_{1-x}Mn_xO_3$ samples at room temperature in the frequency range 10^6–10^9 Hz: (a) real part of permittivity *vs.* frequency; (b) tangent loss *vs.* frequency and (c) complex permittivity plot.

3.4. Magnetic properties

Fig. 9(a) shows the magnetization-field curves $M(H)$ of the $BiFe_{1-x}Mn_xO_3$ ceramics measured at room temperature. Pure $BiFeO_3$ ceramic presents only a small nonlinearity of $M(H)$, without remanent magnetization and almost zero coercivity, typical for the antiferromagnetic behavior. The Mn addition does not fundamentally change the aspect of the magnetization curves, but causes a slight increasing of the magnetization. The low-field magnetic permeability increases with increasing the Mn addition x, as shown in Fig. 9(b). Similar magnetic properties were reported for $BiFe_{1-x}Mn_xO_3$ ceramics prepared by using a wet chemical route [14] or by a solid state reaction method [32].

While $BiFeO_3$ is a canted antiferromagnetic, $BiMnO_3$ is a ferromagnetic as a result of the orbital ordering and superexchange interactions with a low Curie temperature (105 K) [33,34]. At room temperature, by the substitution with magnetic Mn ions on the Fe positions, the G-style spiral magnetic structure existing in pure $BiFeO_3$ is not disturbed by a preferential orientation of spins and consequently, the $BiFe_{1-x}Mn_xO_3$ solid solutions also show at room

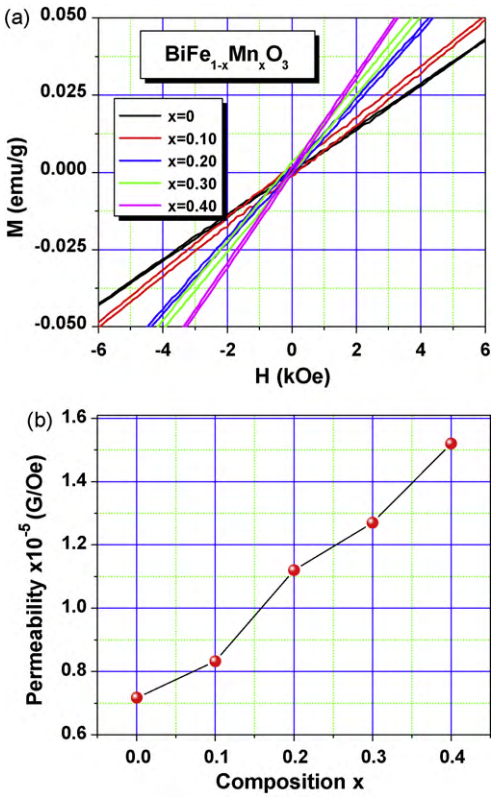

Fig. 9. Magnetic properties of the $BiFe_{1-x}Mn_xO_3$ ($0 \le x \le 0.40$) solid solution at room temperature: (a) $M(H)$ dependence and (b) magnetic permeability *vs.* Mn.

temperature an antiferromagnetic spiral order. It is thus expected that ferromagnetic order will be favored by the presence of Mn in the solid solution $BiFe_{1-x}Mn_xO_3$, but most probably this effect will be stronger in the low-temperature range (not investigated here).

4. Conclusions

In summary, we have studied the effect of Mn substitution in the $BiFeO_3$ ceramics on the dielectric and magnetic behavior. Single phase $BiFe_{1-x}Mn_xO_3$ ceramics were prepared by solid state reaction, involving a two-step thermal treatment procedure (pre-sintering followed by sintering at 850 °C for 2 h, with a heating rate of 5 °C/min). In these conditions, for concentrations $x \le 0.40$, the manganese solute is completely incorporated in the $BiFeO_3$ perovskite lattice. The $BiFe_{1-x}Mn_xO_3$ solid solutions exhibit a hexagonal *R*3c structure. The lattice parameters, the unit cell volume and the crystallite average size obviously decreased with the increasing of the manganese content. From the microstructural point of view, $BiFeO_3$ ceramics exhibit larger grains and a certain intergranular porosity, which affects the sample density. An addition of 10 at% of manganese induces a significant decrease of the average grain size, due to the increase of the amount of the intergranular pores formed by Kirkendall effect. A further increase of the manganese content ($x \ge 0.20$) seems to have a beneficial effect on the densification of the corresponding $BiFe_{1-x}Mn_xO_3$ ceramics.

All the compositions presents a decreasing permittivity with frequency and very high losses (above 1), which seems to be characteristic of a relaxation, conduction behavior and grain boundary phenomena as result of various local amounts of oxygen vacancies. The local electrical inhomogenities are reflected in the complex impedance spectra through the presence of more components, characterized by different relaxation times. At higher frequencies (10^6–10^9) Hz the conductivity and losses reduce and the dielectric properties are acceptable in some range of high frequencies. The intrinsic permittivity at such frequencies are in the range of 10–65. The magnetization at room temperature slightly increases with the Mn substitution, but the antiferromagnetic behavior determined by the $BiFeO_3$ remains prevalent.

Acknowledgement

The financial support of the CNCSIS-PCCEID-76 grant is acknowledged.

References

[1] W. Prellier, M.P. Singh, P. Murugavel, J. Phys.: Condens. Matter 17 (2005) R803–R832.
[2] L. Mitoseriu, Bol. Soc. Esp. Ceram. V. 44 (3) (2005) 177.
[3] N.A. Hill, A. Filippetti, J. Magn. Magn. Mater. 976 (2002) 242–245.
[4] L. Mitoseriu, D. Ricinschi, A. Ianculescu, Multiferroic $BiFeO_3$: Functional properties and possible mechanisms for high polarization, Transworld Research Network 37/661 (2), Fort P.O., Trivandrum, Kerala, India, 2007, pp. 317–338.
[5] P. Fischer, M. Polomska, I. Sosnowska, M. Szymanski, J. Phys. Solid State Phys. 13 (1980) 1931–1940.
[6] Y.K. Jun, W.T. Moon, C.M. Chang, H.S. Kim, H.S. Ryu, J.W. Kim, K.H. Kim, H.S. Hong, Solid State Commun. 135 (2005) 133–137.
[7] S.K. Singh, H. Ishiwara, K. Maruyama, Appl. Phys. Lett. 88 (2006) 262908.
[8] C.F. Chung, J.-P. Lin, J.-M. Wu, Appl. Phys. Lett. 88 (2006) 242909.
[9] X. Qi, J. Dho, R. Tomov, M.G. Blamire, J.L. MacManus-Driscoll, Appl. Phys. Lett. 86 (2005) 62903.
[10] J.K. Kim, S.S. Kim, W.J. Kim, Appl. Phys. Lett. 88 (2006) 132901.
[11] R.D. Shannon, Acta Crystallogr., Sect. A: Cryst. Phys., Diffr., Theor. Gen. Crystallogr. 32 (1976) 751.
[12] I. Sosnowska, M. Lowenhaupt, W.I.F. David, R.M. Ibberson, Physica B 180/181 (1992) 117–118.
[13] H. Naganuma, J. Miura, S. Okamura, Appl. Phys. Lett. 93 (2008) 052901.
[14] V.R. Palkar, C. Darshan, C. Kundaliya, S.K. Malik, J. Appl. Phys. 93 (2003) 4337–4339.
[15] A. Ianculescu, L. Mitoseriu, H. Chiriac, M.M. Carnasciali, A. Braileanu, R. Trusca, J. Optoelectron. Adv. Mater. 10 (2008) 1805–1809.
[16] J.R. Sahu, C.N.R. Rao, Solid State Sci. 9 (2007) 950–954.
[17] A.K. Jonscher, J. Mater. Sci. 16 (1981) 2037.
[18] V.R. Palkar, R. Pinto, Pramana J. Phys. 58 (2002) 1003.
[19] A.S. Poghossian, H.V. Abovian, P.B. Avakian, S.H. Mkrtchian, V.M. Haroutunian, Sens. Actuators B 4 (1991) 545–549.
[20] R. Mazumder, A. Sen, J. Alloys Compounds 475 (2009) 577–580.
[21] G.A. Samara, L.A. Boatner, Phys. Rev. B 61 (2000) 3889.
[22] O. Bidault, M. Maglione, M. Actis, M. Kchikech, B. Salce, Phys. Rev. B 52 (1995) 4191.
[23] C. Ang, Y. Zhi, L.E. Cross, Phys. Rev. B 62 (2000) 228–236.
[24] A.K. Jonscher, Dielectric Relaxation in Solids, Chelsea, Dielectric Press, London, 1983.
[25] A.K. Jonscher, Universal Relaxation Law, Chelsea, Dielectric Press, London, 1996.
[26] I. Bunget, M. Popescu, Physics of Solid Dielectrics, Elsevier, New York, 1978.
[27] H. Wagner, R. Richert, Polymer 38 (1997) 5801.
[28] R. Richert, H. Wagner, Solid State Ionics 105 (1998) 167.
[29] J. Liu, C.G. Duan, W.G. Yin, W.N. Mei, R.W. Smith, J.R. Hardy, J. Chem. Phys. 119 (2003) 2812.
[30] I.M. Hodge, M.D. Ingram, A.R. West, J. Electroanal. Chem. 74 (1976) 125.
[31] R. Gerhardt, J. Phys. Chem. Solids 55 (1994) 1491.
[32] M. Azuma, H. Kanda, A.A. Belik, Y. Shimakawa, M. Takano, J. Magn. Magn. Mater. 310 (2007) 1177–1179.
[33] Z.H. Chi, H. Yang, S.M. Feng, F.Y. Li, R.C. Yu, C.Q. Jin, J. Magn. Magn. Mater. 310 (2007) 358–360.
[34] A. Moreira dos Santos, S. Parashar, A.R. Raju, A.K. Cheetham, C.N.R. Rao, Solid State Commun. 122 (2002) 49–52.